Solanesol derived therapeutic carriers for anticancer drug delivery

Yao Xiong[a,1], Tian Hou[a,1], Lei Liu[a,b,*], Wanjia Peng[a], Chunyun Wang[a], Yan Lu[a], Shuaichao Wang[a], Jiahua Shi[b,*], Shiyong Song[a,*]

[a] *Institute of Pharmacy, School of Pharmacy, Henan University, Kaifeng 475004, China*
[b] *Key Laboratory of Natural Medicine and Immuno-Engineering of Henan Province, Henan University, Kaifeng 475004, China*

ARTICLE INFO

ABSTRACT

Metabolites of a large number of inert drug carriers can cause long-term exogenous biological toxicity. Therefore, carriers with simultaneous therapeutic effects may be a good choice for drug delivery. Herein, a series of pharmacologically active solanesol derivatives were synthesized and investigated for use as micellar drug carriers for cancer therapy. Solanesyl thiosalicylic acid (STS) was first synthesized by introducing a thiosalicylic acid group to solanesol, inspired by the characteristic structure of farnesyl thiosalicylic acid (FTS) which is a non-toxic inhibitor of all active forms of the RAS protein. Then, two amphiphilic derivatives of STS were formed with ester- and hydrazone (HZ)-bond linked methyl poly(ethylene glycol)(mPEG), mPEG-STS and mPEG-HZ-STS, respectively. The PEGylated STS could be formed stable nano-sized micelles loaded with Doxorubicin (DOX). *In vitro*, DOX loaded mPEG-STS and mPEG-HZ-STS micelles exhibited stronger tumor inhibition ability compared with free DOX. *In vivo*, blank mPEG-STS and mPEG-HZ-STS micelles showed an obvious inhibiting effect on tumor growth while the drug loaded micelles had the greatest tumor inhibition effect. The enhanced therapeutic effects and the synergistic effect observed with this solanesol-based drug delivery system could be attributed to the inherent therapeutic qualities of the drug carriers.

1. Introduction

The merits of nano-sized formulations of anticancer drugs have been extensively exploited in the past decades for their potential clinical applications. However, these promising systems face many challenges in transition from bench to bedside. As well as effectiveness, *in vivo* safety should be considered, through studies on the pharmacokinetics, metabolism and pharmacodynamics (Wu and Wang, 2016). In the most cases, carriers are indispensable and inherently inert. The carriers account for a relatively large percentage of the overall therapeutic compound, generally more than 90% by weight. These large quantities of drug-carrier materials as may cause exogenous biological toxicity and related metabolic problems in the body (Chung et al., 2014; Qin et al., 2017a, 2017b, 2017c).

The conflict between the requirement for drug carriers and their potential toxicity can be reduced using multifunctional smart drug delivery systems. To this end, micelle carriers with therapeutic activities have been developed, which could be termed "therapeutic carrier" (Qu et al., 2017; Chu et al., 2016). The application of a therapeutic carrier results in a synergistic anticancer effect between the carrier substance and encapsulated cargos, which can increase the antitumor effect by decreasing the systemic toxicity and even reversing multidrug resistance. A therapeutic carrier can be formed from PEGylated anticancer drugs, which can self-assemble into micelles and encapsulate another drugs (Dong et al., 2012; Li et al., 2009; Zhao et al., 2015). For example, Paclitexal (PTX) were PEGylated to form a polymeric prodrug, PEG-Paclitexal. Paclitexal loaded PEG-Paclitexal micelle formed spherical particles with an averaged size of 100–200 nm, which were more stable and much more effective than PTX loaded other micelles, both *in vitro* and *in vivo* (Lu et al., 2014). Farnesyl thiosalicylic acid (FTS) is a non-toxic inhibitor of all active forms of the Ras protein. FTS has been shown to induce the formation of autophagy in cancer cells, thereby promoting tumor cell death (Schmukler et al., 2013). Li and his coworkers linked two molecules of FTS to a hydrophilic poly(ethylene glycol) (PEG) molecules. The formed conjugate PEG-FTS$_2$ self-assembled to form micelles that could capsulate another therapeutic agents, such as paclitaxel, curcumin. A synergistic antitumor effect was found between PEG-FTS$_2$ and paclitaxel or curcumin. Paclitaxel-loaded PEG-FTS$_2$ micelles showed superior antitumor activity to Taxol (Chen et al., 2014; Zhang et al., 2013). The vitamin E derivative , D-α-

---

tocopherol polyethylene glycol 1000 succinate (TPGS), has been widely used as drug delivery carriers, which can help to stabilize hydrophobic drugs and reverse multidrug resistance by inhibiting P-gylcoprotein (Wang et al., 2015; Tuguntaev et al., 2017; Bao et al., 2014; Han et al., 2015).

Solanesol, which is widely found in tobacco plants such as tobacco and potato, has a variety of pharmacological effects, including antibacterial, anti-inflammatory, anti-tumor, and is used for ulcer treatment (Taylor and Fraser, 2011; Yan et al., 2015). Some derivatives of solanesol were synthesized as anticancer drugs (Wang et al., 2009; Zhao et al., 2004). In our previous work (Qin et al., 2017a, 2017b, 2017c), PEGylated solanesol, solanesyl poly(ethylene glycol) succinate could self-assemble into micelles that encapsulated Coenzyme Q_{10}. The loading content of these micelles could be more than 39% because of the similarity between the solanesol and the coenzyme. In another study (Qin et al., 2017a, 2017b, 2017c), a redox-responsive solanesol derivative, solanesyl poly(ethylene glycol) dithiodipropionate (SPDP), was synthesized and the SPDP micelles showed an accelerated release of loaded Doxorubicin (DOX) in the presence of glutathione. However, the solanesol derivatives including SPGP and SPDP have so little cytotoxicity to tumor cells that the synergistic effect from carriers was limitted.

FTS is derived from a combination of thiosalicylic acid, and farnesol which contains three units of isoprene (Nikolovska-Coleska et al., 2004). The enhanced therapeutic effect of FTS is becaused of the addition thiosalicylate group onto farnesol. Solanesol has nine units of isoprene and almost no toxicity to tumor cells. It was suspected that grafting thiosalicylate onto solanesol would also enhance the therapeutic effect of solanesol. More importantly, micelles formed from solanesol derivative should possess higher stability than the FTS-derived micelles because of the increased length of the hydrophobic chain. In the present study, a solanesol derivative, solanesyl thiosalicylate (STS), was synthesized and found to be more toxic than FTS. Then, STS was PEGylated to form micelle, which could be used as therapeutic carrier for anticancer drugs. In addition, a pH-sensitive hydrazone bond was introduced into the PEGylated STS to enable pH-responsive release of drug. A synergistic effect between the carrier and loaded drugs was also demonstrated through systematic studies *in vitro* and *in vivo*.

2. Materials and methods

2.1. Materials and regents

Solanesol (95%), 4-dimethylaminopyridine (DMAP, 98%), and *N*,*N*'-dicyclohexylcarbodiimide (DCC, 98%) were obtained from Shanghai Darui Fine Chemical Ltd. (Shanghai, China). Methyl poly(ethylene glycol) (mPEG, Mn = 5000 Da) and N-(3-Dimethylaminopropyl)-N′-ethylcarbodiimide hydrochloride (EDC) were purchased from Sigma-Aldrich (Shanghai, China). Doxorubicin hydrochloride (DOX) was purchased from Dalian Meilun Biology Technology Co., Ltd. (Dalian, China). Phosphorus tribromide (PBr₃, 99%), thiosalicylic acid (98%), potassium carbonate (K_2CO_3, 99%), and pyrene (98%) were from JKchemical (Beijing, China). Salirasib (FTS, 98.72%) was provided by MedChemExpress (MCE, USA). 4-Formylbenzoic poly(glycol ethylene) ester (mPEG-CHO) was synthesized according to the previous procedure (Qin et al., 2017a, 2017b, 2017c). The polyclonal rabbit anti-Ras antibody (bs-1515R) was from Bioss (Beijing, China). The polyclonal anti-LC3B antibody (L7543) and autophagy inhibitor chloroquine diphosphate salt (CQ, C6628) were purchased from Sigma-Aldrich (Shanghai, China). The antibodies for P62/SQSTM1 antibody (18420-1-AP) and mouse monoclonal beta actin antibody (60008-1-Ig) were provided by Proteintech (Wuhan, China).

All cells, including human L-02, MCF-7, and HepG-2 cells, were cultured in Roswell Park Memorial Institute (RPMI)-1640 medium supplemented with 10% FBS in a 37 °C incubator with a humidified 5%

CO_2 atmosphere. Fetal bovine serum (FBS) and RPMI-1640 medium were provided by Gibco BRL (MD, USA). 3-(4, 5-Dimethyl-2-thiazolyl)-2,5-diphenyl-2-H-tetrazolium bromide (MTT) and 4′,6-diamidino-2-phenylindole (DAPI) were purchased from Solarbio (Beijing, China).

The experimental Swiss mice (6 weeks old, 20 ± 2 g) were purchased from Henan Experimental Animal Center (Zhengzhou, China). The animal procedures were approved by the animal ethics committee of Henan University and were performed strictly according to the Guide for the Care and Use of Laboratory Animals and the Regulation of Animal Protection Committee.

2.2. Synthesis of solanesyl bromide

Solanesyl bromide was synthesized according to the method previously reported (Marciano et al., 1995). Briefly, solanesol (20 g, 32 mmol) was dissolved in anhydrous petroleum ether (100 mL).After completely dissolved under ultrasonic conditions, pyridine (2.6 mL) was added in it, and PBr₃ (3.6 mL, 13 mmol) was added dropwise slowly with stirring in an ice bath environment. Upon completion of the reaction, pour the distilled water (100 mL), the organic phase was separated and the mixture was centrifuged at 7000–7500 r/min for 5 min. Then some of the organic solvent was removed. The upper layer of light yellow solution was collected. Next, the organic phase was washed with a saturated NaHCO₃ ratio of 1:1 to the organic phase pH 7 ~ 8. Then it was washed twice with saturated brine, dried over anhydrous MgSO₄ and cooled at low temperature to precipitate white crystals. After vacuum filtration and drying, the white product SOL-Br was obtained (yield: 40.3 wt%). The proton nuclear magnetic resonance (^{1}H NMR) spectrum of SOL-Br was characterized by ^{1}H NMR with an AV-400 MHz spectrometer (Bruker, Karlsruhe, Germany), using deuterated chloroform (CDCl₃) as the solvent. ^{1}H NMR (400 MHz, CDCl₃) δ:5.53 (t, 1H, $J = 8.4$ Hz, −CH₂CH₂C=C−H), 5.11 (t, 1H, $J = 7.2$ Hz, CH₃CH₃C=C−H), 4.02 (d, 2H, $J = 8.4$ Hz, −CH₂−Br), 1.98–2.05 (m, 4H, −C=CCH₂CH₂C=C−), 1.68–1.72 (d, 6H, CH₃CH₃C=C−), 1.60 (s, 3H, CH₃−C=C−).

2.3. Synthesis of solanesyl thiosalicylic acid (STS)

The method of synthesis for STS was similar to the procedure for FTS with slight modifications (Zhang et al., 2015). First, solanesyl bromide (4.16 g, 6 mmol) was dissolved in acetone (75 mL) and then cesium carbonate (1.3 g, 7 mmol) and thiosalicylic acid (0.9 g, 6 mmol) were added in sequence, and the mixture was stirred for 24 h at room temperature. The solvent was removed by rotary evaporation. Then, 10 mL chloroform together with 2 drops of HCl (2 M) were added to dissolve the residue. After washing with water, the organic phase was separated and dried with magnesium sulfate. A yellow oily liquid was obtained after the evaporation of the chloroform. This crude product was purified on a silica gel column with chloroform/ethyl acetate (5:1–1:5, v/v), and dried under vacuum at 30 °C for 24 h to provide STS as a faint yellow solid (yield: 87.6 wt%). The structure was verified by infrared spectroscopy, nuclear magnetic resonance (^{1}H NMR), elemental analysis, and mass spectrometry. ^{1}H NMR [400 MHz, deuterated dimethyl sulfoxide (DMSO-*d*)] δ: 5.06 (t, 1H, $J = 7.2$ Hz, −CH₂CH₂C=C−H), 5.26 (t, 1H, $J = 7.2$ Hz, CH₃CH₃C=C−H), 3.55 (d, 2H, $J = 7.52$ Hz, −CH₂−S), 7.18–7.85 (m, 4H, −Ar−H₄), 1.62–1.68 (d, 6H, CH₃CH₃C=C−), 1.92–2.01 (m, 4H, −C=C−CH₂CH₂−C=C−), 1.54 (s, 3H, CH₃−C=C−).

2.4. Synthesis of amphiphilic PEGylated STS (mPEG-STS)

STS (0.5 g, 0.65 mmol), mPEG (Mn:5000 Da) (2.23 g, 0.45 mmol), EDC (0.4 g, 2.1 mmol), DMAP (0.1 g, 0.82 mmol) was dissolved in 50 mL dichloromethane and stirred at room temperature for 24 h. After the removal insoluble matters in the mixture by filtration, the solution was concentrated by evaporation of some of the solvent. The product

was obtained by precipitating the residue solution in ice-cold diethyl ether for twice, followed by vacuum filtration and extensive washing with ethanol. The final product was then dried in a vacuum oven at room temperature (yield: 43.9 wt%). ^{1}H NMR (400 MHz, DMSO-d_6) δ: 5.11 (t, 1H, $J = 7.2$ Hz, −CH$_2$CH$_2$C═C−$\underline{H}$), 5.33 (t, 1H, $J = 7.36$ Hz, CH$_3$CH$_3$C═C−$\underline{H}$),4.65 (t, 2H, $J = 5.6$ Hz, −COOC$\underline{H}_2$), 3.48 (s, 4H, −OC$\underline{H}_2$CH$_2$), 7.2–7.88 (m, 4H, −Ar−$\underline{H}_4$), 3.41 (s, 3H, C$\underline{H}$3−O−), 1.69–1.75 (d, 6H, C$\underline{H}_3$CH$_3$C═C−), 1.99–2.07 (m, 4H, −C═C−C$\underline{H}_2$CH$_2$−C═C−), 1.60 (s, 3H, C$\underline{H}_3$−C═C−).

2.5. Synthesis of hydrazone containing PEGylated STS (mPEG-HZ-STS)

STS (0.5 g, 0.65 mmol), together with hydrazine hydrate (4 mL), was dissolved in 10 mL methanol and the mixture was heated to reflux for 8 h. Solanesyl thiosalicylate hydrazide was obtained after removal of the solvent. Without further purification, the rough product (0.78 g, 1 mmol) was dissolved together with mPEG-CHO (1 g, 0.2 mmol) in 10 mL dichloromethane. The reaction was carried out at 80 °C under reflux for 6 h. After cooling to room temperature, the mixture was filtered and the filtrate was concentrated by rotary evaporation. The final product was obtained by precipitation in 10 × the volume of cold diethyl ether, followed by vacuum filtration, washing and vacuum drying (yield: 53.3 wt%). ^{1}H NMR (400 MHz, DMSO-d_6) δ:5.06 (t, 1H, $J = 7.2$ Hz, −CH$_2$CH$_2$C═C−$\underline{H}$), 5.27 (t, 1H, $J = 6.96$ Hz, CH$_3$CH$_3$C═C−$\underline{H}$), 4.37 (t, 2H, $J = 4.8$ Hz, −COOC$\underline{H}_2$), 3.38 (s, 4H, −OC$\underline{H}_2$CH$_2$), 8.81 (s, 1H, −C$\underline{H}$═N−), 3.36 (s, 3H, C$\underline{H}_3$−O−), 7.16–7.72 (m, 4H, −Ar−$\underline{H}_4$), 7.82–8.11 (m, 4H, −Ar−$\underline{H}_4$), 1.63–1.69 (d, 6H, C$\underline{H}_3$CH$_3$C═C−), 1.93–2.01 (m, 4H, −C═C−C$\underline{H}_2$CH$_2$−C═C−), 1.54 (s, 3H, C$\underline{H}_3$−C═C−).

2.6. Preparation and characterization of blank micelle

Blank micelles were prepared by a solvent evaporation method. Briefly, 1 mL acetone solution containing mPEG-STS (35 mg, 0.006 mmol) or mPEG-HZ-STS (35 mg, 0.0059 mmol) was added dropwise to deionized water (25 mL) and the mixture was stirred at room temperature for 24 h, and filtered through 0.45 and 0.22 μm water filters to obtain a blank micelle solution. The particle size and distribution of the micelles were then measured by a Zeta sizer Nano-ZS90 particle size/zeta potential analyzer (Malvern Instruments, UK). The critical micellar concentration (CMC) values of mPEG-STS and mPEG-HZ-STS were determined on an F-4600 fluorescence spectrometer (Hitachi, Japan) using a pyrene fluorescence probe (Duan et al., 2010).

2.7. Drug loading and release

mPEG-STS (30 mg, 0.005 mmol) or mPEG-HZ-STS (30 mg, 0.005 mmol) were dissolved in acetone (2 mL). Hydrophobic doxorubicin (5 mg) was dissolved in DMSO (2 mL), ultrasonically dissolved in a warm water bath, and mixed with the micelle solution, which was stirred at room temperature for another 2 h. The resulting mixture was added dropwise into 20 mL deionized water to obtain DOX-loaded micelles, which were then dialyzed for 48 h (Molecular Weight Cut Off: 8000). Then, the solution in the dialysis bags was filtered through 0.45 and 0.22 μm filter membranes to remove undissolved DOX. The particle sizes and distributions of DOX-loaded micelles were measured by dynamic light scattering (DLS). Atomic force microscopy (AFM) was used to investigate the morphology of DOX-loaded micelles. To determine the drug-loading capacity (DLC) of the formulations, 2 mg of freeze-dried DOX-loaded micelles (mPEG-STS-DOX, mPEG-HZ-STS-DOX) were dissolved in DMSO, and the content of DOX was determined using a fluorescence spectrophotometer F-4600 (EX: 480 nm; EM: 558 nm) according to the standard curve of a DOX-DMSO solution.

The *in vitro* release profiles of DOX-loaded micelles were recorded in buffers with different pH values. mPEG-STS-DOX or mPEG-HZ-STS-

DOX micelle dispersions (3 mL) were added into dialysis bags (MWCO = 8000–14,000). The bags were then immersed in 40 mL buffer solutions: phosphate buffer (pH 7.4 or 6.5, 0.01 M) or acetate buffer (pH 5.0, 0.01 M), in an incubation shaker at 37 °C at 120 rpm. At certain time intervals, 3 mL of the release medium was collected and another 3 mL of fresh buffer was added. The amount of doxorubicin in the collected samples was measured by a fluorescence spectrophotometer. The release experiments were performed in triplicate and the average values were calculated to obtain a release curve.

2.8. In vitro stability of DOX-loaded micelles

The stability of the DOX-loaded micelles under different conditions, including dilution, plasma, and storage at room temperature, was evaluated by the DLS measurement of size. To investigate the effect of dilution, the DOX-loaded micelles were diluted with different volumes of deionized water. To investigate the stability in plasma, the drug-loaded micelle dry powder (5 mg) was re-dissolved in 10 mL of 1640 medium containing 10% FBS, and then incubated at 37 °C for 48 h with shaking, and samples were taken at 0, 6, 12, 24, and 48 h for particle size measurement. Similarly, the drug-loaded micelle solution was stored at room temperature (25 °C), and the appearance was observed on days 5, 10, 15, 25, and 30, and the particle size distribution was measured to investigate the storage stability of the drug-loaded micelles.

2.9. Cytotoxicity assays

The cytotoxicity of STS, mPEG-STS-DOX, and mPEG-HZ-STS-DOX was evaluated by the MTT assay. MCF-7, HepG-2, (4×10^4 cells per well) were seeded into 96-well plates in 100 μL of 1640 medium with 10% FBS at 37 °C under 5% CO$_2$ humidified atmosphere for 24 h. Then 100 μL of 1640 medium containing different concentration of active compounds, or polymer micelles or DOX loaded micelles were used to replace the old medium. Pure fresh medium and DMSO were used as controls. After incubation for 48 h or 72 h, MTT solution (100 μL, 5 mg/mL) was added to each well and the cells were incubated for another 4 h. The culture supernatant was discarded, and 100 μL of DMSO was added to each well to completely dissolve the formed formazan crystals. The absorbance of each group at 570 nm was measured by a Multiscan Spectrum microplate reader (Thermo Fisher Scientific, USA). The cell viability at each concentration was calculated based on the average absorbance of these experimental groups, and the half-inhibitory concentration (IC$_{50}$) values were calculated by Graphpad Prism 5.0 to examine the cytotoxicity of the samples.

2.10. Laser confocal microscopy

The cellular uptake behavior and the entry of the drugs into the nucleus were investigated using laser confocal microscopy (Carl Zeiss, Germany). HepG2 cells growing in the logarithmic phase were collected and seeded in a six-well plate (1×10^5 cells/well) at 37 °C under a 5% CO$_2$ humidified atmosphere for 24 h. Cells were then treated with mPEG-STS/DOX, mPEG-HZ-STS/DOX, or free DOX for another 12 h. HepG2 cells were washed three times with PBS and fixed with 4% (w/v) paraformaldehyde for 10 min, then the cell nuclei were stained with DAPI. These cells were then washed three times with cold PBS and observed by laser confocal microscopy.

2.11. Western blotting

After being treated with various formulations for 48 h, HepG2 cells in the exponential growth phase were collected and washed three times with pre-cooled PBS. The cells were carefully scraped off with cell scraping and lysed on ice for 30 min. Then, the cells were centrifuged (7170g at 4 °C for 10 min) and the supernatant protein was collected. A

Y. Xiong, et al.

BCA protein assay kit (BOSTER) was used to determine the protein concentration. The protein was separated on a 12% SDS-PAGE gel followed by transfer to a polyvinylidene fluoride membrane. After blocking with 5% skim milk in Tris-buffered saline tween-20 for 1 h, the membranes were then incubated with primary antibodies at 4 °C overnight. Next, the membranes were incubated with horse radish peroxidase (HRP)-labeled secondary antibody at room temperature for 1 h. Excess secondary antibodies were washed away with TBST and protein expression levels were detected by an ECL chemiluminescence kit (Solarbio, China). Actin was used as a control.

2.12. In vivo antitumor efficacy study

The Experimental kunming mice (6 week old, 20 ± 2 g) were purchased from Henan Experimental Animal Center provides (Zhengzhou, China). The animal procedures were approved by the Animal ethics committee of Henan University and were performed strictly according to the Guide for the Care and Use of Laboratory Animals and the Regulation of Animal Protection Committee.

The mice were subcutaneously injected with 1×10^6 H22 cells (in 200 μL PBS) in the right armpit region. When the tumor volume reached 100 mm^3, the mice were randomly divided into eight groups (16 mice per group): (1) saline; (2) FTS (1.5 mg/kg); (3) STS (3.5 mg/kg); (4) DOX (1.25 mg/kg); (5) mPEG-STS (27.75 mg/kg); (6) mPEG-HZ-STS (20.75 mg/kg); (7) mPEG-STS/DOX (1.25 mg/kg DOX); (8) mPEG-HZ-STS/DOX (1.25 mg/kg DOX). The mice were administered these formulations via the tail vein every other day. The mouse body weights and tumor volumes were recorded every day, then the tumor size (V) was calculated using the following formula (Xiao et al., 2015): V = the length × (the width)^2/2.

The tumor inhibition rate (IR) was calculated as follows:

$$IR\,(\%) = (1 - -V_{test}/V_{saline}) \times 100\%$$

After 15 days of administration, the mice were sacrificed on day 16, the primary tumors, and the hearts, livers, spleens, lungs, and kidneys were collected for hematoxylin and eosin (H&E) staining. The apoptosis of the tumor tissues was assessed by the TUNEL assay. Slices were placed under a fluorescence microscope and images were captured.

### 2.13. Statistical analysis

Data are presented as the mean ± SD of three independent experiments. Data were evaluated using GraphPad Prism 5.0 software (GraphPad Software, Inc., San Diego, CA, USA) and statistical analyses were performed by the non-parametric tests. Differences were considered significant when $p < 0.05$.

3. Results and discussion

3.1. Synthesis and characterization of STS and its PEGylation

As shown in Scheme 1, STS was synthesized from solanesol in a two-step manner. Solanesyl bromide was got first by the bromination of solanesol, which was then reacted with thiosalicylic acid in the presence of cesium carbonate as a catalyst. As a result, ^{1}H NMR spectra of solanesol and STS were shown in Fig. 1A and 1B. It could be found that the characteristic peaks of solanesol at δ1.60, δ1.98–2.06, δ5.11, δ5.42, δ4.15 appear on the spectra of both solanesyl bromide and STS. Additionally, the peak at 4.15 ppm, which could be assigned to the proton adjacent to the hydroxyl group on solanesol, shifted to δ 3.5 ppm on the spectra of STS due to the replacement by a thiol group. Typical characteristic peaks of benzene ring in the range of δ 7.2–7.8 ppm were also found in STS ^{1}HNMR spectra. Furthermore, molecular weight of STS was also determined to be 766.79, which is consistent with the theoretical value of 767.25.

The amphiphilic polymers mPEG-STS and mPEG-HZ-STS were then
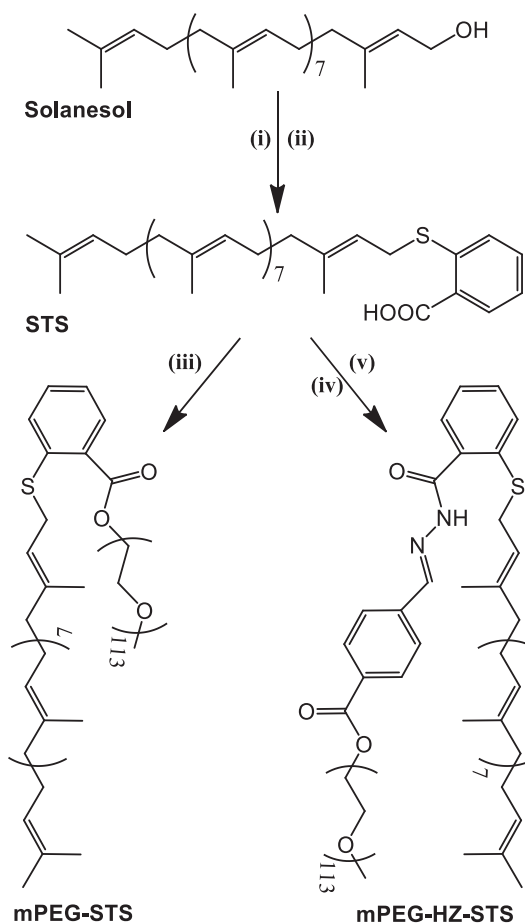
Scheme 1. Synthesis of solanesol derivatives. Reagents and conditions: (i) anhydrous petroleum ether, PBr$_3$, pyridine; (ii) cesium carbonate, thiosalicylic acid, room temperature, 24 h; (iii) DCM, EDC, DMAP, 24 h; (iv) methanol, hydrazine hydrate, 80 °C, 8 h; (v) mPEG-CHO, 80 °C, DCM, 6 h.

synthesized. mPEG-STS was synthesized by a simple esterification reaction between STS and mPEG. mPEG-HZ-STS was prepared in two steps: STS hydrazide was prepared first by the reaction between STS and hydrazine hydrate, followed by the conjugation reaction with mPEG-CHO. The formed hydrazone bond is an acid-labile linkage which endows mPEG-HZ-STS with pH sensitivity. The ^{1}H NMR spectra of mPEG-STS (Fig. 1C) and mPEG-HZ-STS (Fig. 1D) were used to confirm the chemical structures. In Fig. 1C, the peak at δ 4.6 ppm was assigned to the proton of the methylene group adjacent to the formed ester bond, and characteristic signals (δ 3.38–3.82 ppm) of the mPEG moiety in mPEG-STS indicated the successful synthesis of the amphiphilic block polymer mPEG-STS. For mPEG-HZ-STS, peaks corresponding to the protons on a benzene ring (including peaks d, e, 1, 2, 3, and 4 in Fig. 1D) and the peak at δ 4.3 ppm, assigned to the methylene protons adjacent to the ester bond, were observed. In addition, the peak at approximately δ 8.8 ppm was attributed to the hydrazone bond in mPEG-HZ-STS (Qi et al., 2018).

3.2. Formation and characterization of micelles

mPEG-STS and mPEG-HZ-STS could self-assemble into micelles in aqueous solutions. The CMC values of mPEG-STS and mPEG-HZ-STS were determined to be 0.00744 and 0.00764 mg/mL, respectively, using a pyrene fluorescence probe. The relatively low CMC values indicated the high stability of mPEG-STS and mPEG-HZ-STS micelles in aqueous solution. DLS measurements showed that the mPEG-STS and mPEG-HZ-STS micelles had average diameters of 91.63 and 98.55 nm,
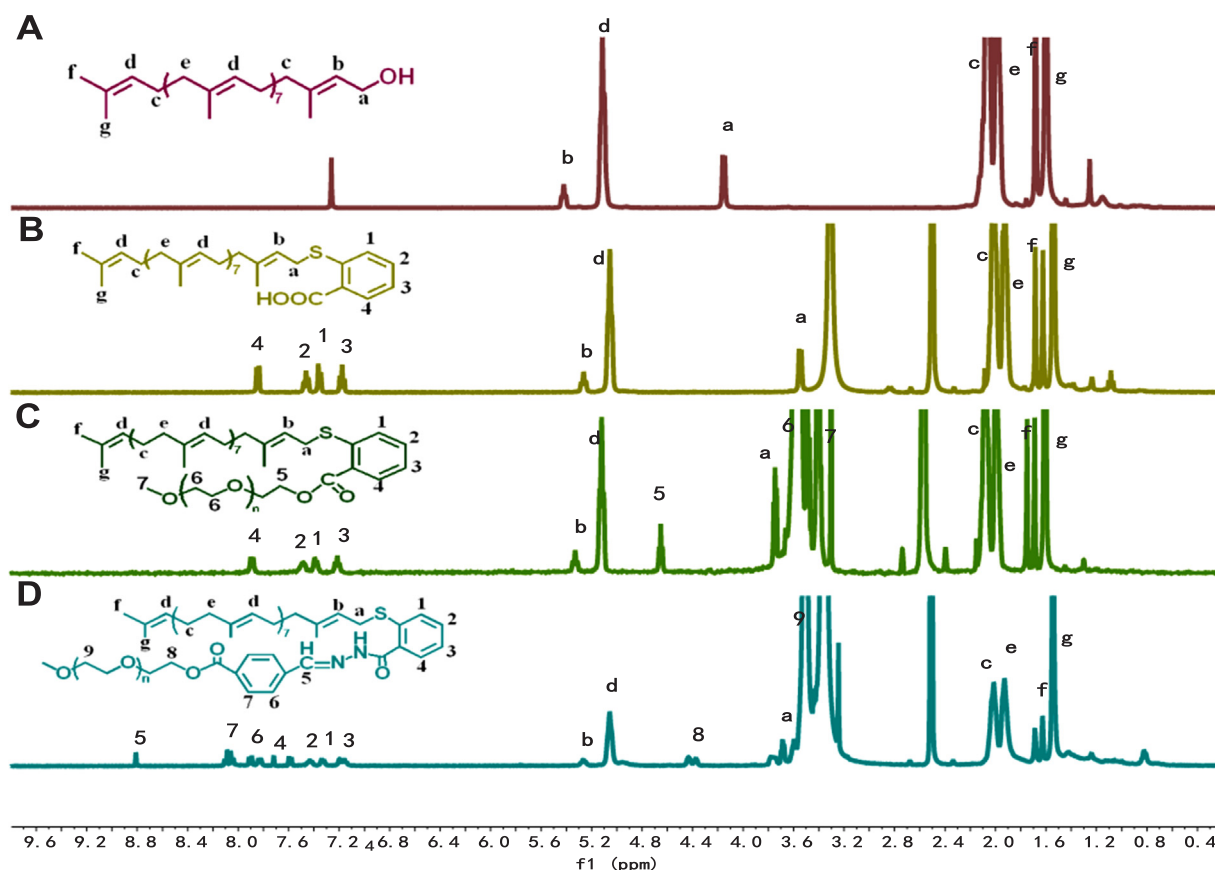
Fig. 1. ^{1}H NMR spectra of the solanesol (A); STS (B); mPEG-STS (C) and mPEG-HZ-STS (D).

respectively. After the loading of DOX, there were obvious increases in size for both micelles. DOX-loaded mPEG-STS micelles (mPEG-STS-DOX) had an average diameter of 118 nm and DOX-loaded mPEG-HZ-STS micelles (mPEG-HZ-STS-DOX) had an average diameter of 129.7 nm. The DLC of mPEG-STS-DOX and mPEG-HZ-STS-DOX were determined to be 4.3% and 5.7%, respectively. The slight increase in the DLC value for mPEG-HZ-STS-DOX might be because of the introduction of the benzene ring-containing hydrazone group in mPEG-HZ-STS. The morphology of the blank micelles and drug-loaded micelles was investigated by TEM (Fig. 2). TEM images showed that they were spherical nanoparticles with sizes smaller than DLS ones100 nm, which may be due to shrinkage of the PEG layer caused by shrinkage during drying, but the PEG layer in aqueous solution is fully stretched with a hydration layer. The pH responsive degradation of mPEG-HZ-STS-DOX micelles were also investigated by DLS measurements and TEM (Fig. S1). After 12 h incubation in an acidic solution (pH 5.0), the bigger particles with an averaged diameter above 200 nm were formed. Incubated for 36 h large clusters were visible in the TEM images and obvious participation were found in the solution. That is because the micelles degraded into pieces in acidic condition and the hydrophobic species aggregated to form bigger particles. The micelle solutions will be diluted in the bloodstream after administration via intravenous injection and will need to hold their integrity in the bloodstream. The dilution stability of the micelles was assessed based on the evolution of size under different dilution conditions (Fig. 3). It was found that the micelle formulations showed excellent stability up to nearly 500-fold dilution. While the PDI values for each formulation varied from 0.1 to 0.7 (Fig. S2), indicating a relative uniformly distributed sizes. It was also found that most PDI for each formulation increased with dilution. So, the dilution slightly disturbed structure of the micelles. The particle sizes showed no obvious changes along with a slight increase in the distribution of size. The size of the DOX-loaded micelles changed less

than the blank micelles under the same dilution conditions. The increase in hydrophobic–hydrophobic interactions by the incorporation of DOX should stabilize the micelle structure. This increased stability of the drug-loaded micelles is beneficial in prolonging the circulation time.

In addition to the dissociation of micelles, the interference of proteins in the bloodstream is another cause for failure of micellar formulations of drugs. The change in size of the drug-loaded micelles in a medium containing 10% fetal bovine serum was monitored by DLS for 48 h. As shown in Fig. 4A, the size of the two drug-loaded micelles remained unchanged, indicating that no appreciable protein adsorption occurred, and the micelles had excellent stability. The good plasma stability is because of the hydrophilic shell of the micelle structure (mPEG), which can protect easily degradable groups (esters, amides, and lactones), effectively reducing the adsorption of plasma proteins and resulting in long circulation times *in vivo*. In addition, mPEG-STS-DOX and mPEG-HZ-STS-DOX in aqueous solution showed no obvious changes over a month at 25 °C (Fig. 4B).

3.3. In vitro release study

The drug-release behavior of mPEG-STS-DOX and mPEG-HZ-STS-DOX micelles in solutions with different pH values were investigated (Fig. 6). mPEG-HZ-STS contains a hydrazone bond, which is more pH sensitive than the ester bond in mPEG-STS. As a result, more pH-sensitive release behavior was found for mPEG-HZ-STS-DOX. As shown in Fig. 5A, in a solution at pH 7.4, DOX release from mPEG-STS-DOX was slow and reached a maximum of less than 30% in approximately 12 h. A slight acceleration in DOX release was found in acidic conditions; the lower the pH, the faster the release. The slight pH dependence of the release of DOX from mPEG-STS-DOX could be attributed to the nature of DOX. The protonation of DOX in acidic conditions will enhance the
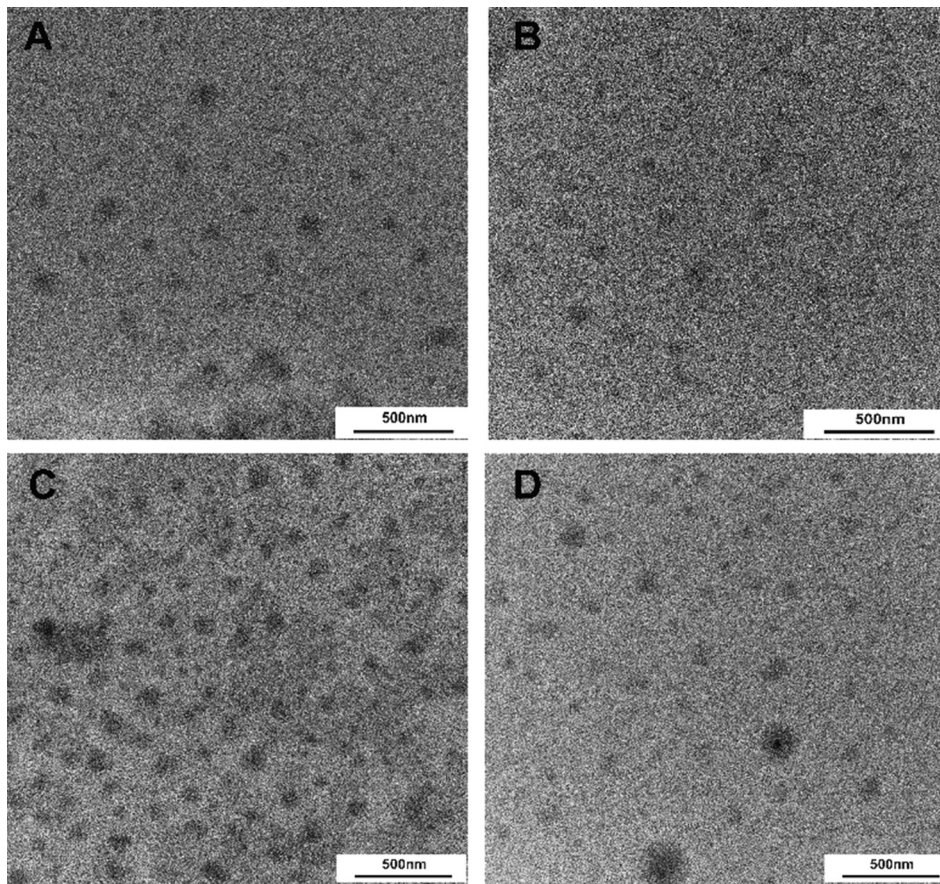
Y. Xiong, et al.

Fig. 2. Observation on the morphology of blank micelles and drug-loaded micelles by transmission electron microscopy (TEM): mPEG-STS (A); mPEG-HZ-STS (B); mPEG –STS-DOX (C) and mPEG-HZ-STS-DOX (D).
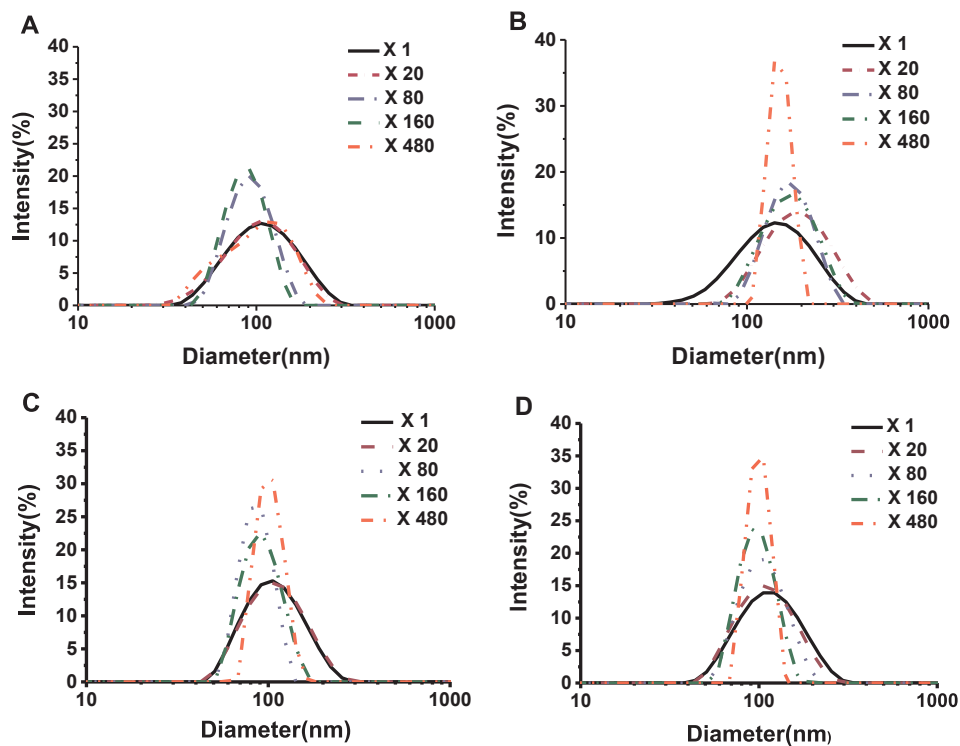

Fig. 3. Size evolution of micelles under different dilution folds in volume: mPEG-STS (A), mPEG-HZ-STS (B), mPEG-STS-DOX (C) and mPEG-HZ-STS-DOX (D).
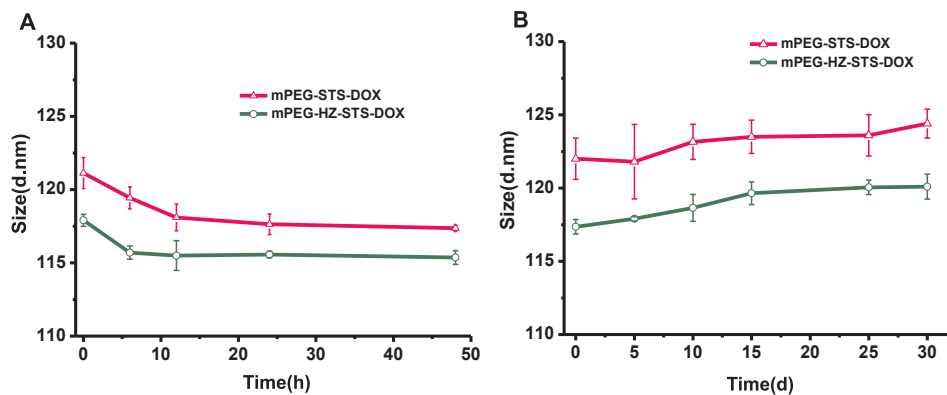
Fig. 4. Evolutions in sizes of drug loaded micelles at 37 °C in plasma solution (A) and at 25 °C in aqueous solution (B).
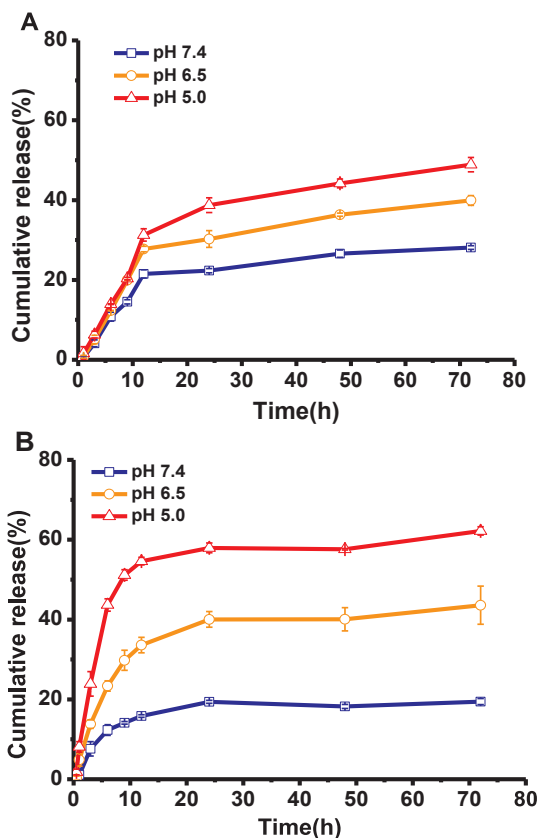

Fig. 5. Release profile of drug-loaded micelles at different pH conditions: mPEG-STS -DOX (A) and mPEG-HZ-STS -DOX (B).
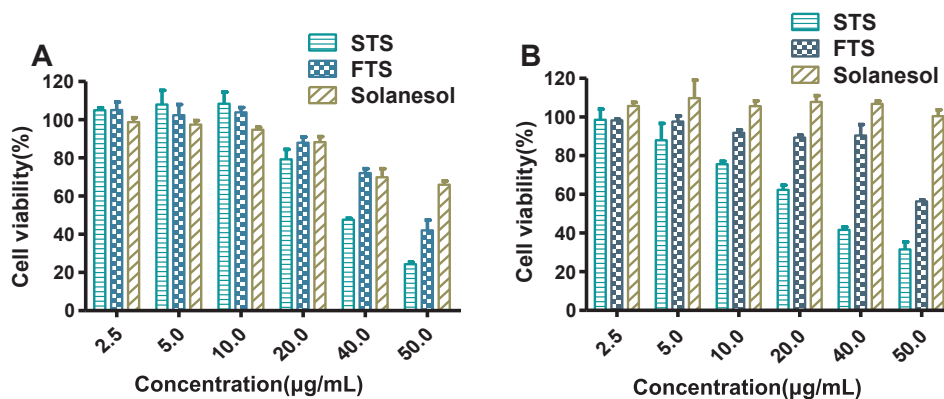
water solubility and then promote the release of DOX. Even under acidic conditions, the maximum release rate was less than 50% over 72 h. Greater pH-sensitive drug release was found for mPEG-HZ-STS-DOX (Fig. 5B). At pH 7.4, the release of DOX was even slower than that of mPEG- STS-DOX. This slow release might result from the higher affinity between DOX and mPEG-HZ-STS, which is consistent with the results of DLC. At pH 6.5, more than 30% DOX was released from mPEG-HZ-STS-DOX in the first 10 h. At pH 5.0, more than 50% DOX was released in the first 10 h and approximately 63% release was reached in 72 h. It is likely that the pH-sensitive hydrazone bond in the mPEG-HZ-STS micelles led to the accelerated release of DOX in acidic conditions. The cleavage of the hydrazone bond in an acidic environment destroyed the micelle structure, leading to the accelerated release of DOX (Xu et al., 2016; Prabaharan et al., 2009).

3.4. Cytotoxicity of STS and PEGylated STS micelles

The cytotoxicity of STS was first determined because STS was designed to be the therapeutic part of the therapeutic carrier. As shown in Fig. 6, solanesol has low toxicity to both HepG2 and MCF-7 cells. Even at a dosage of 50 μg/mL, solanesol had almost no cytotoxic effect on MCF-7 cells. FTS (Salirasib) inhibited the proliferation of HepG2 and MCF-7 cells in a dose-dependent manner with average IC_{50} values of 47.36 and 61.26 μM, respectively. STS was found to be more toxic than FTS and had lower IC_{50} values of 36.21 (HepG2) and 28.52 μM (MCF-7). The solanesyl group in STS endows STS with enhanced affinity to the phospholipid bilayer membrane of cells compared with FTS. Furthermore, the longer hydrophobic chain of STS is the key to forming a stable micelle. The PEGylated STS could self-assemble into micelles in aqueous solutions.

Subsequently, the cytotoxicity of mPEG-STS and mPEG-HZ-STS micelles were evaluated toward HepG-2 and MCF-7 cells. After
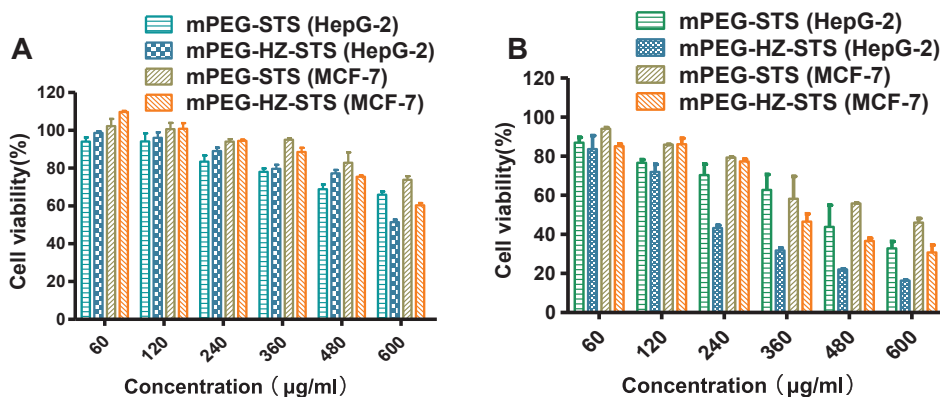

Fig. 6. Cytotoxicity of STS, FTS and Solanesol towards HepG-2 cells (A) and MCF-7 cells (B) in 48 h.

Fig. 7. Cytotoxicity of mPEG-STS micelles and mPEG-HZ-STS micelles towards HepG-2 cells and MCF-7 cells for 48 h (A) and 72 h (B).

culturing for 48 h, the PEGylated STS micelles had almost no toxicity to HepG2 and MCF-7 cells at low dosage (Fig. 7A) (Yoo et al., 2017). Even at a high concentrations of 600 μg/mL, more than 50% of the tumor cells remained, which was more than for STS. Thus, the PEGylation of STS sharply decreased the cytotoxicity. The mPEG-HZ-STS micelles were shown to be more toxic than the mPEG-STS micelles in both tumor cell lines. A prolonged incubation time of 72 h resulted in greater tumor cell death, and the mPEG-HZ-STS micelles were more toxic (Fig. 7B). The longer the incubation time, the greater the observed toxicity, which might be because, over longer incubation periods, more STS detached from the mPEG. The hydrazone-containing mPEG-HZ-STS micelles could release the STS moiety more quickly under acidic conditions than the ester-containing mPEG-STS micelles (Ding et al., 2015).

mPEG-HZ-STS and mPEG-STS micelles were also used to encapsulate DOX and the cytotoxicity was evaluated. As indicated in Fig. 8, free DOX was the most cytotoxic to HepG2 and MCF-7 cells under any conditions. Doxorubicin is a small molecule that can rapidly penetrate through the cell membrane and enter into the nucleus by

passive diffusion, while the drug-loaded micelles can only enter cells and release DOX by endocytosis because of their high molecular weights (Sun et al., 2010; Qiu et al., 2014, 2011).

The cytotoxicity of the drug-loaded micelles mPEG-HZ-STS-DOX was greater than for the mPEG-STS-DOX micelles because of the pH sensitivity of mPEG-HZ-STS-DOX. The faster release of DOX and the STS therapeutic moiety may be involved in the greater cytotoxicity of mPEG-HZ-STS-DOX. After incubation for 72 h, the difference in cytotoxicity between the drug-loaded micelles and free DOX decreased. In particular, for the higher doses of DOX in MCF-7 cells, all the compounds had almost equal effects on tumor cells. Unfortunately, a synergistic effect between the therapeutic carriers and the encapsulated DOX was not obvious in this case, which may because of the great differences in the cytotoxicity. The 48-h IC_{50} values of DOX, mPEG-HZ-STS, and mPEG-STS micelles were calculated to be 0.684, 672, and 1053.0 μg/mL, respectively. DOX plays a predominant role in the cytotoxicity. Therefore, the effect of the mPEG-HZ-STS and mPEG-STS micelles was negligible in these circumstances. Even so, STS had
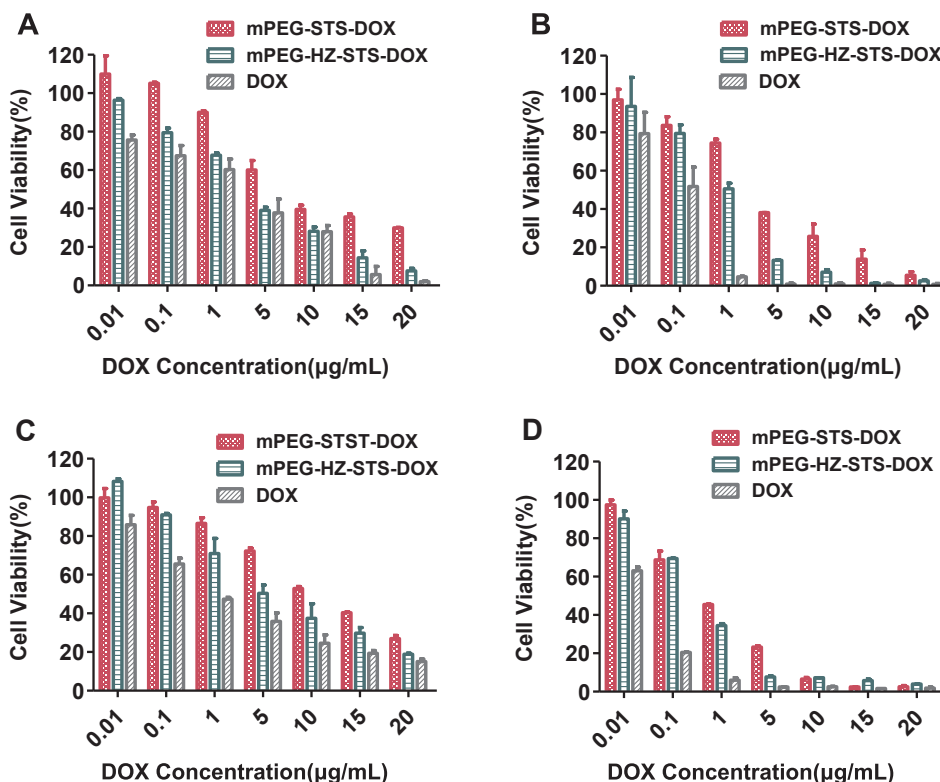

Fig. 8. Inhibition of the activity of DOX loaded micelles and free DOX on HepG-2 cells (A: 48 h, B: 72 h) and MCF-7 cells (C: 48 h, D: 72 h).
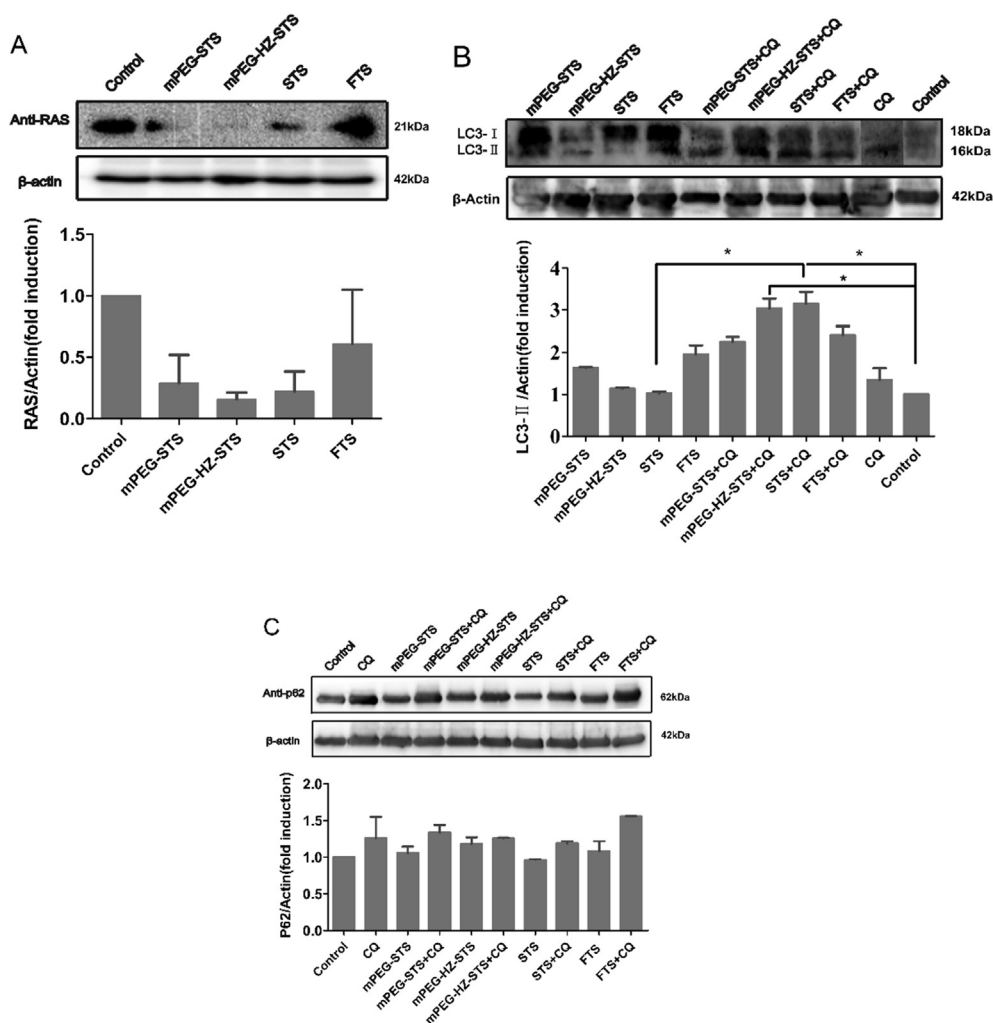
Fig. 9. FTS and SOL-based carrier materials induce RAS-mediated autophagy in HepG2 cells treated with or without autophagy inhibitor CQ(50 mM). (A) The treated HepG2 cells with FTS (40ug/mL), STS (40ug/mL), mPEG-STS (400ug/mL) and mPEG-HZ-STS (400ug/mL) were subjected to immunoblot analysis using RAS. The treated cells were subjected to immunoblot analysis using (B) LC3 and (C) P62 in the presence or absence of CQ. Quantitative analysis of RAS, LC3 and P62 protein levels using Image J software. No treatment group was used as a control group (*p < 0.05, **p < 0.01, ***p < 0.001).

smaller IC_{50} values of 36.21 and 28.52 µg/mL toward HepG2 and MCF-7 cells, respectively, after 48 h, compared with the values for the micelles. *In vivo* synergistic effects between the drug and STS-based micelles should be expected.

3.5. Western blotting

To further investigate the effects of the solanesol derivatives on tumor suppression and autophagy, the expression levels of RAS, LC3, and P62 in HepG2 cells were determined in the presence or absence of autophagy inhibitors. FTS has been extensively studied as a non-toxic RAS inhibitor, which inhibits the methylation of RAS and downregulates active RAS-GTP (Faigenbaum et al., 2013). In this study, the FTS group was used as a positive control group.

Western blot analysis showed that the synthesized STS, mPEG-STS, and mPEG-HZ-STS obviously reduced the expression of RAS in HepG2 cells, compared with the FTS group, (Fig. 9A). The reason for this result may be that STS has three isoprene units, similar to the isoprene moiety of FTS, which is a mimic of *trans*-farnesyl-L-cysteine (AFC). AFC specifically binds to the RAS farnesyl cysteine region and inhibits RAS methylation (Marom et al., 1995), resulting in a decrease in RAS levels on the cell membrane and decreased cell growth depending on where the RAS is inhibited. Notably, the materials we synthesized contained a longer isoprene structure, which increases the hydrophobicity and

makes it easier for the compounds to bind to proteins (Maltese, 1990). mPEG-HZ-STS showed the lowest RAS protein level, consistent with the enhanced cytotoxicity results for mPEG-HZ-STS caused by the pH sensitivity of the hydrazone bond.

The link between autophagy and RAS is complicated. Ras can regulate the level of autophagy in cancer cells, and autophagy may affect the progression of Ras-driven tumors. Autophagy is negatively regulated by mTOR inhibition of phosphorylation of Atg1 and Atg13. In addtition, RAS acts as a positive regulator of the class I PI3K/Akt/mTOR1 pathway and acts as a negative regulator of autophagy (Schmukler et al., 2015). Autophagy can also be activated by the RAS-regulated Raf-1/MEK1/2/ERK pathway (Wu et al., 2015). The western blotting results indicated that RAS can be effectively inhibited by FTS and synthetic STS, mPEG-STS, mPEG-HZ-STS. Fig. 9B further shows that FTS promoted the accumulation of LC3-II compared with the blank control (Expressed as the ratio of LC3-II to actin instead of LC3-I). Similarly, the synthetic mPEG-STS and mPEG-HZ-STS also slightly increased the level of LC3-II, indicating the formation of autophagosomes and the promotion of autophagy. Inhibition of RAS can promote autophagy, which has an impact on the death of tumor cells.

Increased autophagosome formation causes accumulation of LC3-II, but this accumulation can also occur if the autophagosome-lysosome fusion is impaired (Sarkar et al., 2007). HepG2 cells were treated with FTS, STS, mPEG-STS, or mPEG-HZ-STS for 24 h in the presence of the
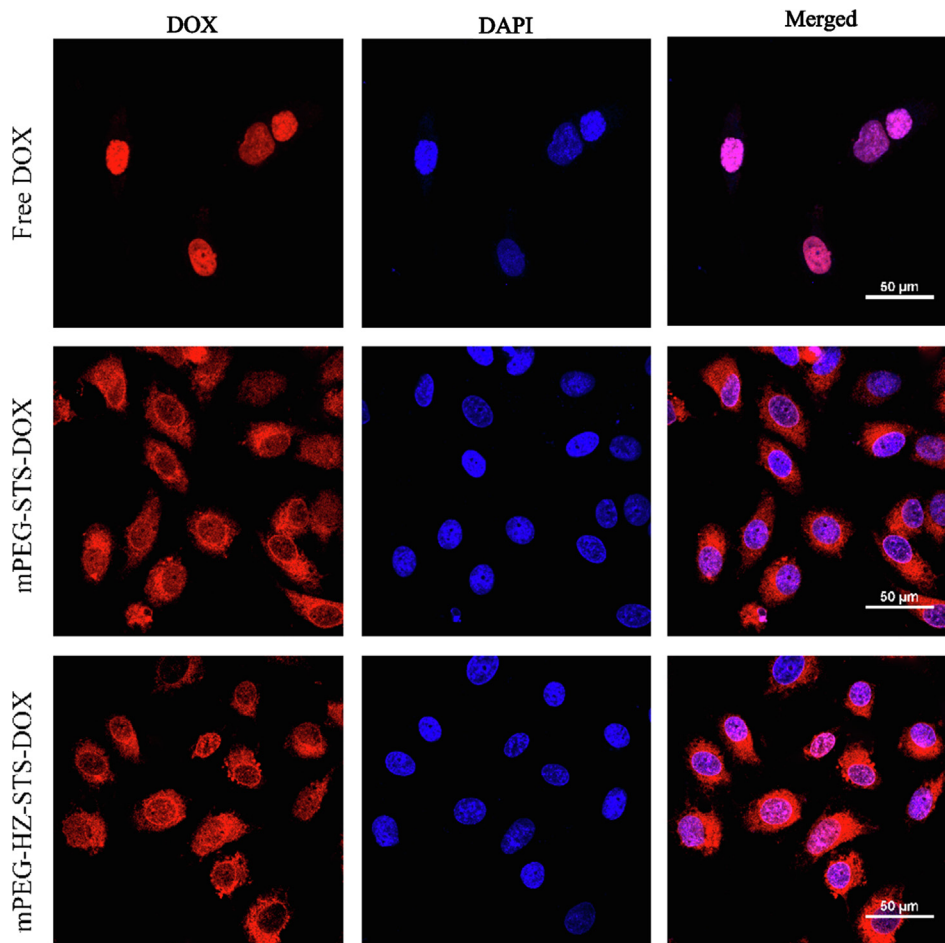
Fig. 10. CLSM images of HepG2 cells after 12 h incubation with free DOX, mPEG-STS-DOX and mPEG-HZ-STS-DOX .(DOX concentration is 15 mg/L and scale bar indicates 50 μm).
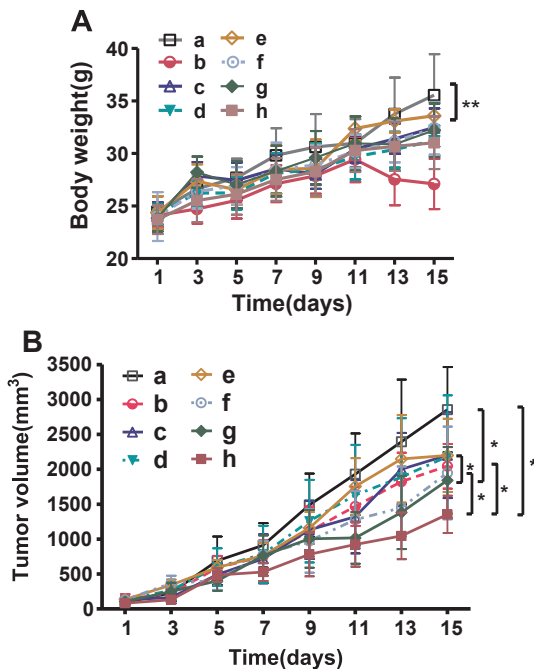

Fig. 11. Weight changes (A) and tumor volume changes of H22 tumor-bearing mice treated with different formulations: (a) Saline, (b) Free DOX, (c) STS, (d) FTS, (e) mPEG–STS, (f) mPEG-HZ-STS, (g) mPEG–STS-DOX and (h) mPEG-HZ-STS-DOX. (*p < 0.05,**p < 0.01, ***p < 0.001).

late-stage autophagy inhibitor CQ (Rubinsztein et al., 2007; Boya et al., 2005) (Fig. 9B and C), which itself is weakly alkaline, can destroy the acidic environment of lysosomes, inhibit the activity of lysosomal enzymes and make autophagosomes unable to be degraded and accumulate. The expression level of LC3-II (expressed as the ratio of LC3-II to actin instead of LC3-I) in the CQ-alone treatment group was increased compared with the blank control group, but was much lower than that of the solanesol derivative groups in combination with the inhibitor CQ, demonstrating that the solanesol derivatives promoted the synthesis of autophagosomes. This result was confirmed when P62 was also further elevated in the presence of autophagy inhibitors (Fig. 9C and F). In summary, the solanesol derivatives, including mPEG-STS and mPEG-HZ-STS, which have the same effect as FTS, can promote the formation of autophagosomes, and have an important influence on the survival of tumor cells.

3.6. Intracellular uptake

To further verify the effect of the STS micelles as drug carriers for drug delivery, the intracellular uptake and release behavior of free DOX and the drug-loaded micelles in HepG2 cells were observed by laser confocal microscopy (Fig. 10). The free DOX group displayed strong red fluorescence in the nucleus because doxorubicin is a small molecule, which can passively diffuse through the cell membrane and enter the nucleus (Li et al., 2014). The fluorescence intensity values were also acquired from the images. As is shown below (Fig. S3), the fluorescence intensity among the three group had no significant difference. So, from the result, one could not tell which formulation was faster but only

confirm the successful internalization.

3.7. In vivo antitumor activity

The tumor growth inhibition ability of the STS-based therapeutic carriers was investigated in a H22 subcutaneous tumor model. As shown in Fig. 11A, except for the free DOX group, all the groups showed slight increases in body weight (p < 0.01), indicating negligible toxicity to the system. As shown in Fig. 11B, the tumor volume of the saline group was nearly 3000 mm^3. The groups treated with the drugs showed an obvious decrease in tumor volumes. STS had comparable tumor inhibition ability with free DOX and FTS *in vivo*. The PEGylation of STS did not result in any obvious reduction in tumor volume, which is in contrast with the *in vitro* results. The hydrazone-containing STS derivative showed a slightly increased antitumor ability. Impressively, the DOX-loaded micelles, mPEG-STS-DOX and mPEG-HZ-STS-DOX, exhibited better antitumor effects than both free DOX and the blank micelles, which indicated a synergistic therapeutic effect in the H22 tumor model was achieved by encapsulating DOX into the STS-based therapeutic carriers. This effect was more obvious in the mPEG-HZ-STS-DOX group because the pH-sensitive nature of mPEG-HZ-STS-DOX resulted in the destruction of the micelle structure triggering the simultaneous release of STS and DOX.

3.8. Histopathological and immunohistological analysis

To further confirm the anti-tumor effect and tissue toxicity of the various formulations, H&E staining and TUNEL tests were carried out on tumors (Fig. 12). The H&E staining showed that the saline group had densely distributed tumor cells with normal morphology. However, varying degrees of necrotic areas were found in the drug-treated
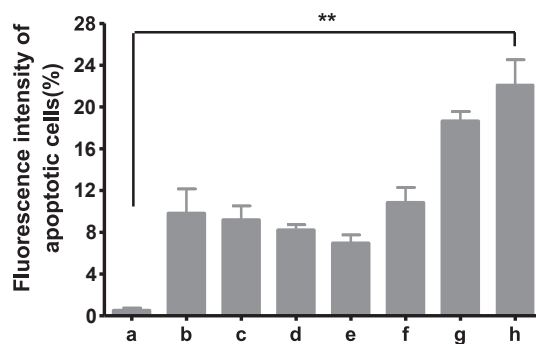

Fig. 13. Quantification of the apoptotic fluorescence intensity of tumor cells in TUNEL assay. (a) Saline, (b) Free DOX, (c) STS, (d) FTS, (e) mPEG–STS, (f) mPEG-HZ-STS, (g) mPEG –STS-DOX and (h) mPEG-HZ-STS-DOX.

groups, where a large number of cells without a cell nucleus, deep nuclear staining, and cytoplasmic condensation were found, suggesting that the tumor cells had undergone apoptosis. Notably, mPEG-HZ-STS-DOX-treated tumors showed the lowest density of tumor cells, as well as ruptured areas.

Accordingly, mPEG-STS-DOX- also induced a marked change in the microstructure of tumor cells. For the TUNEL analysis (Figs. 12 and 13), the tumor treated with mPEG-HZ-STS-DOX showed the strongest FITC green fluorescence, an indicative signal of tumor cell apoptosis. There was almost no green fluorescence in the saline group. STS induced more apoptosis of tumor cell than FTS, which is consistent with the *in vitro* results. mPEG-HZ-STS was more toxic than mPEG–STS because of the acid-cleavable nature of hydrazone bond. As for mPEG–STS, the PEGylation increased the solubility in water but decreased the cytotoxicity
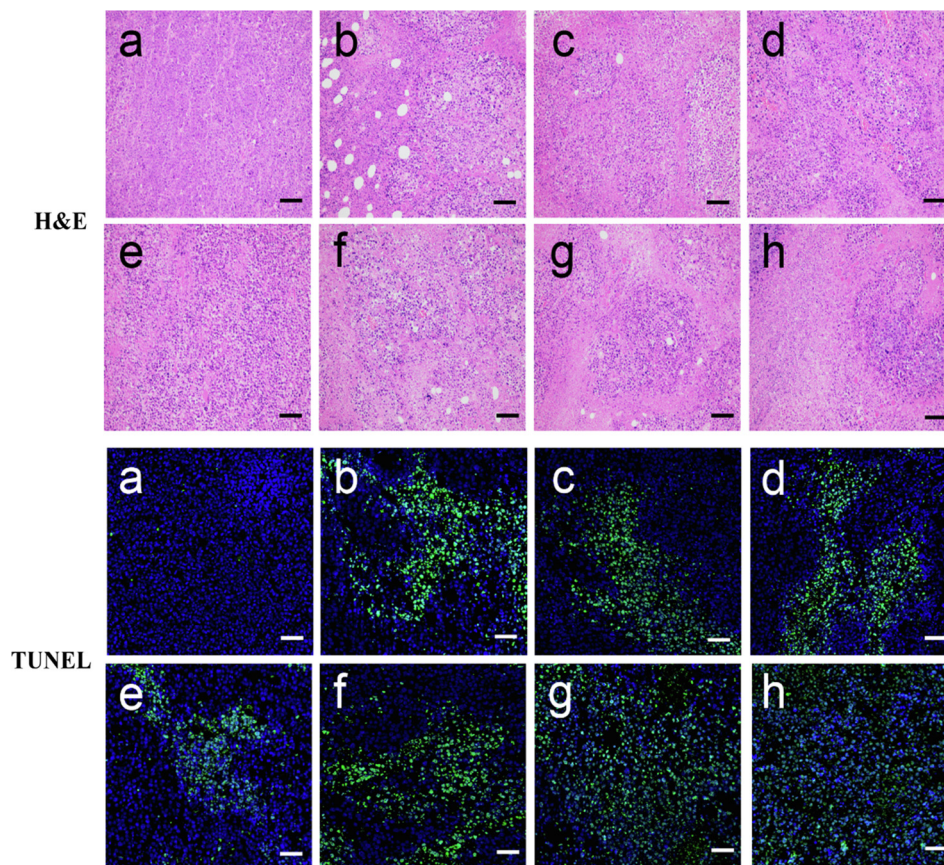

Fig. 12. Images of Histological assay and TUNEL assay of tumor from H22 tumor-bearing mice treated with different formulations: (a) Saline, (b) Free DOX, (c) STS, (d) FTS, (e) mPEG –STS, (f) mPEG-HZ-STS, (g) mPEG-STS-DOX and (h) mPEG-HZ-STS-DOX. (Scale bar indicates 5 µm).

of STS. By introducing pH sensitive bond, another PEGylation form of STS, mPEG-HZ-STS, not only increased the solubility but also the cytotoxicity.

4. Conclusion

An active carrier platform was constructed based on the natural product solanesol, which self-assembled to form micelles for the delivery of the anticancer drug DOX. In the case of STS, the tumor cell survival rate was significantly reduced and the level of RAS protein was also reduced. The amphiphilic mPEG-STS micelles were constructed to efficiently load DOX and the acid-triggered drug release of the micelles was realized by the incorporation of a hydrazone bond. The formed mPEG-derived STS micelle structures alleviated the cytotoxicity caused by STS, but long-term culture caused the destruction of the micelle structures, and the link between mPEG and STS was broken, thereby releasing the active group STS to function synergistically with the drug. In addition, mPEG-derived STS micelles effectively reduced the expression levels of oncogene RAS and induced the occurrence of autophagy negatively regulated by the RAS signaling pathway. *In vivo* experiments also confirmed that mPEG-derived STS micelles effectively inhibited tumor growth. The pharmacologically active solanesol derivatives were used to construct a novel drug-loading system for delivering anti-tumor drugs, which acted like the combination of the drugs for tumor treatment. The mechanism of the synergistic anti-tumor effect should be evaluated in future studies.

Funding

Declaration of Competing Interest

The authors declare that they have no known competing financial interests or personal relationships that could have appeared to influence the work reported in this paper.

Appendix A. Supplementary material

Supplementary data to this article can be found online at https://doi.org/10.1016/j.ijpharm.2019.118823.

References

Bao, Y., Guo, Y., Zhuang, X., Li, D., Cheng, B., Tan, S., Zhang, Z., 2014. D-α-tocopherol polyethylene glycol succinate-based redox-sensitive paclitaxel prodrug for overcoming multidrug resistance in cancer cells. Mol. Pharm. 11, 3196–3209. https://doi.org/10.1021/mp500384d.

Boya, P., Rosa-Ana Casares, Gonzalez-Polo, N., Perfettini, J., Dessen, P., Larochette, N., Métivier, D., Meley, D., Souquere, S., Yoshimori, T., Pierron, G., Codogno, P., Kroemer, G., 2005. Inhibition of Macroautophagy Triggers Apoptosis Inhibition of Macroautophagy Triggers Apoptosis. Mol. Cell. Biol. 25, 1025–1040. https://doi.org/10.1128/MCB.25.3.1025.

Chu, B., Qu, Y., Huang, Y., Zhang, L., Chen, X., Long, C., He, Y., Ou, C., Qian, Z., 2016. PEG-derivatized octacosanol as micellar carrier for paclitaxel delivery. Int. J. Pharm. 500, 345–359. https://doi.org/10.1016/j.ijpharm.2016.01.030.

Chung, J.E., Tan, S., Gao, S.J., Yongvongsoontorn, N., Kim, S.H., Lee, J.H., Choi, H.S., Yano, H., Zhuo, L., Kurisawa, M., Ying, J.Y., 2014. Self-assembled micellar nanocomplexes comprising green tea catechin derivatives and protein drugs for cancer therapy. Nat. Nanotechnol. 9, 907–912. https://doi.org/10.1038/nnano.2014.208.

Chen, Y., Zhang, X., Lu, J., Huang, Y., Li, J., Li, S., 2014. Targeted delivery of curcumin to tumors via PEG-derivatized FTS-based micellar system. AAPS J. 16, 600–608. https://doi.org/10.1208/s12248-014-9595-6.

Dong, H., Dong, C., Feng, Y., Ren, T., Zhang, Z., Li, L., Li, Y., 2012. Engineering of peglayted camptothecin into core-shell nanomicelles for improving solubility, stability and combination delivery. MedChemComm 3, 1555–1561. https://doi.org/10.1039/c2md20153d.

Duan, K., Zhang, X., Tang, X., Yu, J., Liu, S., Wang, D., Li, Y., Huang, J., 2010. Fabrication of cationic nanomicelle from chitosan-graft-polycaprolactone as the carrier of 7-ethyl-10-hydroxy-camptothecin. Colloids Surf. B Biointerf. 76, 475–482. https://doi.org/10.1016/j.colsurfb.2009.12.007.

Ding, Y., Sun, D., Wang, G.L., Yang, H.G., Xu, H.F., Chen, J.H., Xie, Y., Wang, Z.Q., 2015. An efficient PEGylated liposomal nanocarrier containing cell-penetrating peptide and pH-sensitive hydrazone bond for enhancing tumor-targeted drug delivery. Int. J. Nanomedicine 10, 6199–6214. https://doi.org/10.2147/IJN.S92519.

Faigenbaum, R., Haklai, R., Ben-Baruch, G., Kloog, Y., 2013. Growth of poorly differentiated endometrial carcinoma is inhibited by combined action of medroxyprogesterone acetate and the Ras inhibitor Salirasib. Oncotarget 4, 316–328. https://doi.org/10.18632/oncotarget.867.

Han, N., Zhao, Q., Wan, L., Wang, Y., Gao, Y., Wang, P., Wang, Z., Zhang, J., Jiang, T., Wang, S., 2015. Hybrid lipid-capped mesoporous silica for stimuli-responsive drug release and overcoming multidrug resistance. ACS Appl. Mater. Interfaces 7, 3342–3351. https://doi.org/10.1021/am5082793.

Lu, J., Chuan, X., Zhang, H., Dai, W., Wang, Xinglin, Wang, Xueqing, Zhang, Q., 2014. Free paclitaxel loaded PEGylated-paclitaxel nanoparticles: preparation and comparison with other paclitaxel systems in vitro and in vivo. Int. J. Pharm. 471, 525–535. https://doi.org/10.1016/j.ijpharm.2014.05.032.

Li, J., Wang, Y., Yang, C., Wang, M., Oelschlager, D.K., Zheng, Y., Tian, D.-A., Grizzle, W.E., Buchsbaum, D.J., Wan, M., 2009. Polyethylene glycosylated curcumin conjugate inhibits pancreatic cancer cell growth through inactivation of Jab1. Mol. Pharmacol. 76, 81–90. https://doi.org/10.1124/mol.109.054551.

Li, Ning, Li, Na., Yi, Q., Luo, K., Guo, C., Pan, D., Gu, Z., 2014. Amphiphilic peptide dendritic copolymer-doxorubicin nanoscale conjugate self-assembled to enzyme-responsive anti-cancer agent. Biomaterials 35, 9529–9545. https://doi.org/10.1016/j.biomaterials.2014.07.059.

Marciano, D., Ben-Baruch, G., Marom, M., Egozi, Y., Haklai, R., Kloog, Y., 1995. Farnesyl derivatives of rigid carboxylic acids-inhibitors of ras-dependent cell growth. J. Med. Chem. 38, 1267–1272. https://doi.org/10.1021/jm00008a004.

Marom, M., Haklai, R., Ben-Baruch, G., Marciano, D., Egozi, Y., Kloog, Y., 1995. Selective inhibition of ras-dependent cell growth by farnesylthiosalisylic acid. J. Biol. Chem. 270, 22263–22270. https://doi.org/10.1074/jbc.270.38.22263.

Maltese, W.A., 1990. Posttranslational modification of proteins by isoprenoids in mammalian cells. Faseb J. 4, 3319–3328. https://doi.org/10.1096/fasebj.4.15.2123808.

Nikolovska-Coleska, Z., Xu, L., Hu, Z., Tomita, Y., Li, P., Roller, P.P., Wang, R., Fang, X., Guo, R., Zhang, M., Lippman, M.E., Yang, D., Wang, S., 2004. Discovery of embelin as a cell-permeable, small-molecular weight inhibitor of XIAP through structure-based computational screening of a traditional herbal medicine three-dimensional structure database. J. Med. Chem. 47, 2430–2440. https://doi.org/10.1021/jm030420+.

Prabaharan, M., Grailer, J.J., Pilla, S., Steeber, D.A., Gong, S., 2009. Amphiphilic multi-arm-block copolymer conjugated with doxorubicin via pH-sensitive hydrazone bond for tumor-targeted drug delivery. Biomaterials 30, 5757–5766. https://doi.org/10.1016/j.biomaterials.2009.07.020.

Qin, S.Y., Zhang, A.Q., Cheng, S.X., Rong, L., Zhang, X.Z., 2017a. Drug self-delivery systems for cancer therapy. Biomaterials 112, 234–247. https://doi.org/10.1016/j.biomaterials.2016.10.016.

Qu, Y., Chu, B.Y., Shi, K., Peng, J.R., Qian, Z.Y., 2017. Recent progress in functional micellar carriers with intrinsic therapeutic activities for anticancer drug delivery. J. Biomed. Nanotechnol. 13, 1598–1618. https://doi.org/10.1166/jbn.2017.2475.

Qin, B., Liu, L., Pan, Y., Zhu, Y., Wu, X., Song, S., Han, G., 2017b. PEGylated Solanesol for Oral Delivery of Coenzyme Q 10. J. Agric. Food Chem. 65, 3360–3367. https://doi.org/10.1021/acs.jafc.7b00165.

Qin, B., Liu, L., Wu, X., Liang, F., Hou, T., Pan, Y., Song, S., 2017c. mPEGylated solanesol micelles as redox-responsive nanocarriers with synergistic anticancer effect. Acta Biomater. 64, 211–222. https://doi.org/10.1016/j.actbio.2017.09.040.

Qi, P., Wu, X., Liu, L., Yu, H., Song, S., 2018. Hydrazone-containing triblock copolymeric micelles for pH-controlled drug delivery. Front. Pharmacol. 9, 1–11. https://doi.org/10.3389/fphar.2018.00012.

Qiu, F., Wang, D., Zhu, Q., Zhu, L., Tong, G., Lu, Y., Yan, D., Zhu, X., 2014. Real-time monitoring of anticancer drug release with highly fluorescent star-conjugated copolymer as a drug carrier. Biomacromolecules 15, 1355–1364. https://doi.org/10.1021/bm401891c.

Qiu, F., Tu, C., Wang, R., Zhu, L., Chen, Y., Tong, G., Zhu, B., He, L., Yan, D., Zhu, X., 2011. Emission enhancement of conjugated polymers through self-assembly of unimolecular micelles to multi-micelle aggregates. Chem. Commun. 47, 9678–9680. https://doi.org/10.1039/c1cc13587b.

Rubinsztein, D.C., Gestwicki, J.E., Murphy, L.O., Klionsky, D.J., 2007. Potential therapeutic applications of autophagy. Nat. Rev. Drug Discov. https://doi.org/10.1038/nrd2272.

Schmukler, E., Wolfson, E., Haklai, R., Sfadia, G.E., Kloog, Y., Kramarski, R.P., 2013. Chloroquine synergizes with FTS to enhance cell growth inhibition and cell death. Oncotarget 5, 173–184. https://doi.org/10.18632/oncotarget.1500.

Sun, H., Guo, B., Li, X., Cheng, R., Meng, F., Liu, H., Zhong, Z., 2010. Shell-sheddable micelles based on dextran-SS-poly(ε-caprolactone) diblock copolymer for efficient intracellular release of doxorubicin. Biomacromolecules 11, 848–854. https://doi.org/10.1021/bm1001069.

Schmukler, E., Kloog, Y., Pinkas-Kramarski, R., 2015. Ras and autophagy in cancer development and therapy. Oncotarget 5, 577–586. https://doi.org/10.18632/oncotarget.1775.

Sarkar, S., Davies, J.E., Huang, Z., Tunnacliffe, A., Rubinsztein, D.C., 2007. Trehalose, a novel mTOR-independent autophagy enhancer, accelerates the clearance of mutant huntingtin and α-synuclein. J. Biol. Chem. 282, 5641–5652. https://doi.org/10.1074/jbc.M609532200.

Tuguntaev, R.G., Chen, S., Eltahan, A.S., Mozhi, A., Jin, S., Zhang, J., Li, C., Wang, P.C.,

Liang, X.J., 2017. P-gp inhibition and mitochondrial impairment by dual-functional nanostructure based on vitamin e derivatives to overcome multidrug resistance. ACS Appl. Mater. Interfaces 9, 16900–16912. https://doi.org/10.1021/acsami.7b03877.

Taylor, M.A., Fraser, P.D., 2011. Solanesol: added value from solanaceous waste. Phytochemistry 72, 1323–1327. https://doi.org/10.1016/j.phytochem.2011.03.015.

Wu, H.Q., Wang, C.C., 2016. Biodegradable smart nanogels: a new platform for targeting drug delivery and biomedical diagnostics. Langmuir 32, 6211–6225. https://doi.org/10.1021/acs.langmuir.6b00842.

Wang, A.T., Liang, D.S., Liu, Y.J., Qi, X.R., 2015. Roles of ligand and TPGS of micelles in regulating internalization, penetration and accumulation against sensitive or resistant tumor and therapy for multidrug resistant tumors. Biomaterials 53, 160–172. https://doi.org/10.1016/j.biomaterials.2015.02.077.

Wang, J.H., Gao, R.H., Gan, Y., Xie, S.Q., Wang, C.J., Zhao, J., 2009. Synthesis and evaluation of solanesol derivatives as novel potent synergistic agents. J. Asian Nat. Prod. Res. 11, 978–984. https://doi.org/10.1080/10286020903313098.

Wu, S.-Y., Lan, S.-H., Cheng, D.-E., Chen, W.-K., Shen, C.-H., Lee, Y.-R., Zuchini, R., Liu, H.-S., 2015. Ras-related tumorigenesis is suppressed by BNIP3-mediated autophagy through inhibition of cell proliferation. Neoplasia 13, 1171-IN28. https://doi.org/10.1593/neo.11888.

Xiao, K., Li, Y.P., Wang, C., Ahmad, S., Vu, M., Kuma, K., Cheng, Y.Q., Lam, K.S., 2015. Disulfide cross-linked micelles of novel HDAC inhibitor thailandepsin A for the treatment of breast cancer. Biomaterials 67, 183–193. https://doi.org/10.1016/j.biomaterials.2015.07.033.

Xu, J., Luan, S., Qin, B., Wang, Y., Wang, K., Qi, P., Song, S., 2016. Backbone-hydrazone-containing biodegradable copolymeric micelles for anticancer drug delivery. J. Nanopart. Res. 18. https://doi.org/10.1007/s11051-016-3626-4.

Yan, N., Liu, Y., Gong, D., Du, Y., Zhang, H., Zhang, Z., 2015. Solanesol: a review of its resources, derivatives, bioactivities, medicinal applications, and biosynthesis. Phytochem. Rev. 14, 403–417. https://doi.org/10.1007/s11101-015-9393-5.

Yoo, J., Sanoj Rejinold, N., Lee, D.Y., Jon, S., Kim, Y.C., 2017. Protease-activatable cell-penetrating peptide possessing ROS-triggered phase transition for enhanced cancer therapy. J. Control. Release 264, 89–101. https://doi.org/10.1016/j.jconrel.2017.08.026.

Zhao, D., Liu, N., Shi, K., Wang, X., Wu, G., 2015. Preparation of a multifunctional verapamil-loaded nano-carrier based on a self-assembling PEGylated prodrug. Colloids Surf. B Biointerfaces 135, 682–688. https://doi.org/10.1016/j.colsurfb.2015.08.018.

Zhang, X., Lu, J., Huang, Y., Zhao, W., Chen, Y., Li, J., Gao, X., Venkataramanan, R., Sun, M., Stolz, D.B., 2013. PEG-farnesylthiosalicylate conjugate as a nanomicellar carrier for delivery of paclitaxel. Bioconjug Chem. 24, 464–472. https://doi.org/10.1021/bc300608h.

Zhao, J., Liu, L., Song, J., Wang, C., 2004. Synthesis and biological activity of glycosyl N-solanesylaminocarboxylic esters. Chin. J. Org. Chem. 24, 1601–1605.

Zhang, X., Huang, Y., Ghazwani, M., Zhang, P., Li, J., Thorne, S.H., Li, S., 2015. Tunable pH-responsive polymeric micelle for cancer treatment. ACS Macro Lett. 4, 620–623. https://doi.org/10.1021/acsmacrolett.5b00165.